Draft version January 26, 2011
Preprint typeset using LaTeX style emulateapj v. 6/6/04

SUCCESSIVE MERGING OF PLASMOIDS AND FRAGMENTATION IN FLARE CURRENT SHEET AND THEIR X-RAY AND RADIO SIGNATURES

Marian Karlický[1] and Miroslav Bárta[1,2]
[1]Astronomical Institute of the Academy of Sciences of the Czech Republic, CZ-25165 Ondřejov, Czech Republic
[2]Max Planck Institute for Solar System Research, D-37191 Katlenburg-Lindau, Germany

Draft version January 26, 2011

ABSTRACT

Based on our recent MHD simulations, first, a concept of the successive merging of plasmoids and fragmentation in the current sheet in the standard flare model is presented. Then, using a 2.5-D electromagnetic particle-in-cell model with free boundary conditions, these processes were modelled on the kinetic level of plasma description. We recognized the plasmoids which mutually interacted and finally merged into one large plasmoid. Between interacting plasmoids further plasmoids and current sheets on smaller and smaller spatial scales were formed in agreement with the fragmentation found in MHD simulations. During interactions (merging - coalescences) of the plasmoids the electrons were very efficiently accelerated and heated. We found that after a series of such merging processes the electrons in some regions reached the energies relevant for the emission in the hard X-ray range. Considering these energetic electrons and assuming the plasma density 10^9–10^{10} cm^{-3} and the source volume as in the December 31, 2007 flare (Krucker at al. 2010), we computed the X-ray spectra as produced by the bremsstrahlung emission process. Comparing these spectra with observations, we think that these processes can explain the observed above-the-loop-top hard X-ray sources. Furthermore, we show that the process of a fragmentation between two merging plasmoids can generate the narrowband dm-spikes. Formulas for schematic fractal reconnection structures were derived. Finally, the results were discussed.

Subject headings: Plasmas — Solar flares — Acceleration of particles

1. INTRODUCTION

It is commonly accepted that plasmoids play a very important role in the magnetic field reconnection in solar flares. Their importance, for the first time, was recognized by Ohyama & Shibata (1998). In the 1992 October 5 flare, observed in soft X-rays by *Yohkoh* satellite, they analyzed the plasmoid which was ejected during the impulsive phase upwards into the corona. Studying the same flare, Kliem et al. (2000) showed that this plasmoid ejection was associated with the drifting pulsating structure (DPS) on radiowaves. They proposed the model of this radio emission, which was further developed in the papers by Karlický et al. (2002), Karlický (2004), Karlický & Bárta (2007), Bárta et al. (2008a), and Karlický et al. (2010). In this model, in the current sheet, due to tearing and coalescence processes the plasmoids are formed. As shown by Drake et al. (2005, 2006), Hoshino (2005), Pritchett (2006, 2008), and Karlický (2008) during these processes electrons are very efficiently accelerated. The electrons are then trapped in plasmoids, where they generate Langmuir waves, which through a wave transformation produce the electromagnetic waves recorded on the radio spectrum as DPSs. Due to limited range of plasma densities in the plasmoid the DPS is generated in the limited range of frequencies. In the vertical current sheet the plasmoids move upwards or downwards or even stay without any motion in dependance on a form of the surrounding magnetic field (Bárta et al. 2008a,b). Due to a preference of divergent magnetic field lines in the upward direction, most of the plasmoids move upwards and corresponding DPSs drift towards lower frequencies. Nevertheless, in some cases the plasmoids move downwards and even interact with the underlying flare arcade as observed by Kolomanski & Karlický (2007) and Milligan et al. (2010).

Recently, Oka et al. (2010) studied the electron acceleration by multi-island coalescence processes in PIC model with periodic boundary conditions. They found that the most effective acceleration process is during the coalescence of plasmoids ("anti-reconnection"), see also Pritchett (2008) and Karlický & Bárta (2007).

Furthermore, Shibata & Tanuma (2001) proposed that the current sheet, stretched by a rising magnetic rope, is fragmented to smaller and smaller plasmoids by the tearing mode instability in subsequently narrower and narrower current sheets (cascading reconnection). This suggestion has been recently further theoretically developed by Loureiro et al. (2007) and Uzdensky et al. (2010) into the theory of chain plasmoid instability. An advantage of this concept is that it explains how very narrow current sheets with high current densities (requested for the anomalous resistivity generation and fast reconnection) are generated. Moreover, many X-points in this model give sufficient volume for an acceleration of particles.

Besides this fragmentation described by Shibata & Tanuma (2001), Bárta et al. (2010b) found a new fragmentation in the region between two merging plasmoids using MHD simulations. This fragmentation is caused by the tearing mode instability in the current sheet generated between these interacting plasmoids and this process is repeated in smaller and smaller spatial scales. This fragmentation is driven by a merging process of the plasmoids.

Electronic address: karlicky@asu.cas.cz

Considering all the above-mentioned processes, in the present paper, we focus our attention to two processes: (a) successive merging of plasmoids to large plasmoid and (b) fragmentation process between merging plasmoids. We selected these processes because we think that the successive merging of plasmoids can explain the above-the-loop-top hard X-ray source (as a large stationary plasmoid). On the other hand, the fragmentation can explain the narrowband dm-spikes. Because both these phenomena are generated by accelerated electrons, in following simulations we use the particle-in-cell (PIC) model instead of MHD models (e.g. Bárta et al. 2008a,b).

The above-the-loop-top hard X-ray sources belong to the most discussed topics in recent years. The well-known example of such a hard X-ray source is that observed in the ∼30–50 keV energy range by Masuda et al. (1994). However, such events are very rare (Tomczak 2001; Petrosian et al. 2002; Krucker & Lin 2008). Another very interesting example was published just recently by Krucker et al. (2010). They presented the hard X-ray source (with the energy up to ∼80 keV) which was located 6 Mm above thermal flare loops. They derived the upper limit of the plasma density and source volume as $n_e \sim 8\times10^9$ cm^{-3} and $V \sim 8\times 10^{26}$ cm^3, respectively. Just a relatively low plasma density in such hard X-ray sources attracts attention of scientists. Krucker et al. (2010) concluded that these hard X-ray sources have to be close to the acceleration region and the distribution function of electrons emitting hard X-rays is strongly non-thermal or the plasma in the source is very hot (up to $T_e \sim 200$ MK). Several ideas explaining these X-ray sources have been proposed, e.g. the magnetic or turbulent trapping, and dense (collisionally thick) coronal sources (see Fletcher 1995; Jakimiec et al. 1998; Veronig & Brown 2004; Park & Fleishman 2010)

The narrowband dm-spikes (further spikes) belong to the most interesting radio bursts due to exceptionally high brightness temperatures ($T_b \approx 10^{15}$ K) and short durations (≤ 0.1 s, see the review by Benz 1986). Their observational characteristics were described in many papers (e.g. Slottje 1981; Karlický 1984; Fu et al. 1985; Stähli & Magun 1986; Benz et al. 1982; Zlobec & Karlický 1998; Mészárosová et al. 2003). On the other hand, the theoretical models can be divided into two groups: a) based on the plasma emission and acceleration processes (Kuijpers et al. 1981; Tajima et al. 1990; Wentzel 1991; Bárta & Karlický 2001), and b) based on the electron-cyclotron maser (Holman et al. 1980; Melrose & Dulk 1982; Vlahos & Sharma 1984; Winglee et al. 1988; Aschwanden 1990; Fleishman & Yastrebov 1994). To distinguish between these two types of models polarization and harmonic structures of the spikes have been also studied (Güdel 1990; Güdel & Zlobec 1991; Krucker & Benz 1994). Searching for a characteristic bandwidth of individual spikes Karlický et al. (1996, 2000) found that the Fourier transform of the dynamic spectra of spikes have a power-law form with power-law indices close to $-5/3$. Based on these results Bárta & Karlický (2001) proposed that the spikes are generated in turbulent reconnection outflows.

This paper is organized as follows: First, we present our model scenario and explain the successive merging and fragmentation process. Then using a 2.5-D PIC model we simulate these processes. The results are then used in the interpretation of the above-the-loop-top hard X-ray sources and narrowband dm-spikes.

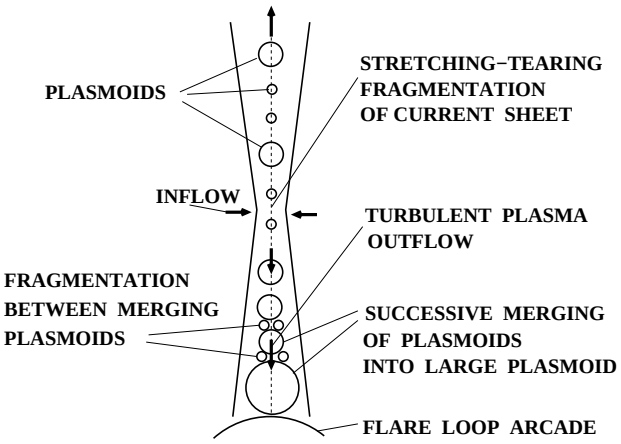

FIG. 1.— Model scenario.

2. MODEL SCENARIO AND SIMULATION MODEL

Fig. 1 shows our model scenario, which is based on the 'standard' CSHKP flare model (e.g. Magara et al. 1996, and references therein). In the central part of the current sheet, in agreement with Shibata & Tanuma (2001), we assume a fragmentation of the current sheet (stretching-tearing fragmentation). Furthermore, based on the new results of Bárta et al. (2010b), we propose that the reconnection plasma outflow (which is downward oriented) accumulates plasmoids in the region just above the flare arcade, where thus plasmoids can interact efficiently. We think that in some cases a large plasmoid can be formed here as a result of successive merging of plasmoids. On the other hand, between the merging plasmoids new current sheets are formed and in these current sheets one again further (but on smaller and smaller spatial scales) plasmoids are generated (fragmentation between merging plasmoids). While the first process of the successive merging we propose for the interpretation of the above-the-loop-top hard X-ray sources, the second process is a very promising process explaining the narrowband dm-spikes (see the following sections 3.1 and 3.2).

For simulation we used a 2.5-D (2D3V – 2 spatial and 3 velocity components) fully relativistic electromagnetic particle-in-cell model (Saito & Sakai 2004; Karlický 2004). The system size is $L_x \times L_y = 600\Delta \times 4000\Delta$, where Δ (=1) is a grid size. The current sheet is initiated along the line $x = 0\Delta$, and its half-width is $L = 10\Delta$. In this first study we consider the neutral current sheet, i.e. the guiding magnetic field B_z is zero. Thus, the initial magnetic field is:

$$\begin{aligned} \mathbf{B} &\equiv (B_x, B_y, B_z), \\ B_y &= -B_0 \text{ for } x < -L, \\ B_y &= xB_0/L \text{ for } -L \leq x \leq +L, \\ B_y &= B_0 \text{ for } x > +L, \\ B_x &= 0, B_z = 0. \end{aligned}$$

The electron-proton plasma with the proton-electron

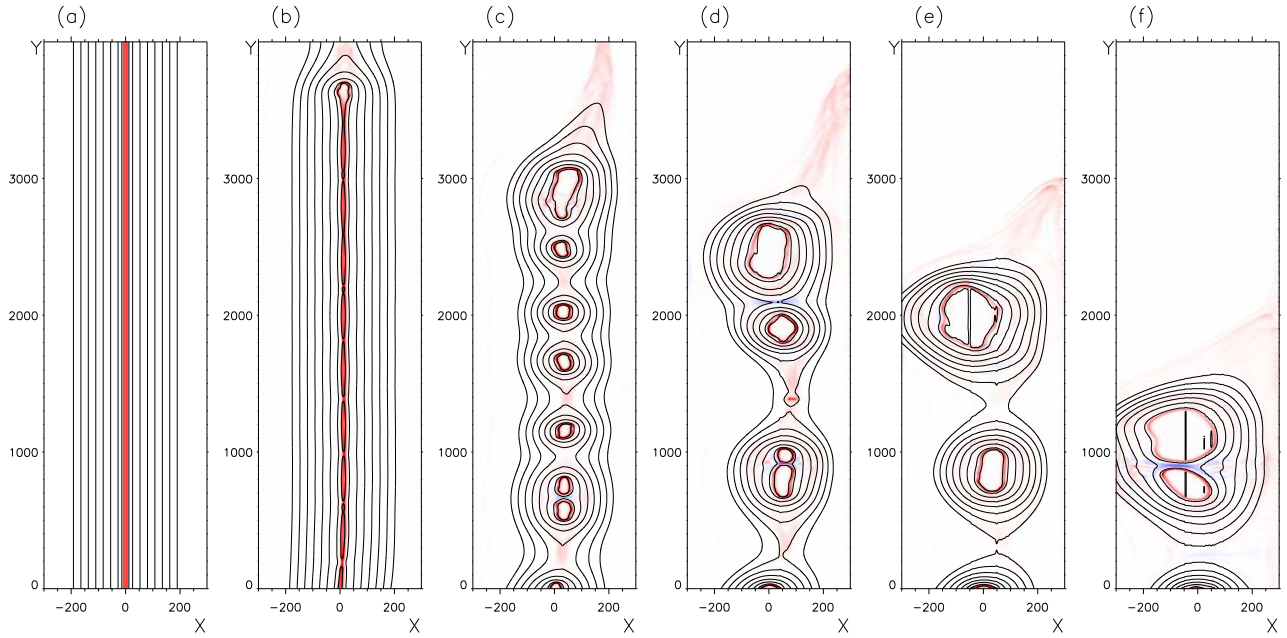

FIG. 2.— The global view on magnetic field lines and corresponding current densities (reddish areas) in the $x-y$ computational plane at six different times: at the initial state (a), at $\omega_{pe}t = 1200$ (b), at $\omega_{pe}t = 2500$ (c), at $\omega_{pe}t = 3500$ (d), at $\omega_{pe}t = 4500$ (e), and at $\omega_{pe}t = 6500$ (f). The x and y coordinates are expressed in Δ. The proton inertial length is 40 Δ.

mass ratio m_p/m_e=16 is unrealistic, but taken here to shorten computations. Nevertheless, the electron mass is low enough to separate the dynamics of electrons and protons well. In each numerical cell located outside of the current sheet, we initiated $n_0 = 60$ electrons and $n_0 = 60$ protons. In the current sheet the initial number density was enhanced just to keep the pressure equilibrium. The initial electron temperature was taken to be the same in the whole numerical box as T = 10 MK and the temperature of protons was chosen the same as electrons. The plasma frequency is $\omega_{pe}\Delta t = 0.05$ (Δt is the time step which equals to 1), the electron Debye length is $\lambda_D = 0.6\ \Delta$, and the electron and proton inertial lengths are $d_e = 10\ \Delta$ and $d_i = 40\ \Delta$, respectively. To study successive coalescence processes among several plasmoids, we initiated a formation of 10 plasmoids along the current sheet by a cosine perturbation of the electric current density in the sheet; with the k-vector $k = 2\pi \cdot 10/4000 = 0.0157\ \Delta^{-1}$ and the amplitude corresponding to the current density $\mathbf{j}$ given by the magnetic field in the current sheet ($\boldsymbol{j} = \boldsymbol{\nabla} \times \boldsymbol{B}$). We made computations with several initial values of the plasma β parameter. Here, we present the results with $\beta = 0.07$. It gives the ratio of the plasma densities in the centrum and out of the current sheet as 15.3. The free boundary conditions were used. All computations were performed on the parallel computer OCAS (Ondřejov Cluster for Astrophysical Simulations), see http://wave.asu.cas.cz/ocas.

3. RESULTS

A global evolution of the magnetic field lines and the corresponding electric current densities (reddish areas) in the system is shown in Fig. 2. When 10 small plasmoids were formed, at about $\omega_{pe}t = 1200$ (Fig. 2b), then the plasmoids started to interact and merge into larger plasmoids. Due to free boundaries used in the system and small asymmetries in the initiation, the plasmoids successively merged into one large plasmoid formed in the bottom part of the system (Fig. 2f). On the other hand, Fig. 3 presents a more detailed view on this evolution as well as the distribution of numerical electrons (points), having the energy greater than 40 keV, at four different times: at $\omega_{pe}t = 3200$ (a), at $\omega_{pe}t = 3500$ (b), at $\omega_{pe}t = 5600$ (c), and at $\omega_{pe}t = 7800$ (d). As can be seen here, in each coalescence process electrons are very efficiently accelerated – see an increase of the number of numerical electrons in dependence on time. In Fig. 3b and 3d, we selected the region (see white crosses = the centra of the circles of the radius 70 Δ) with an enhanced number of accelerated electrons. In these regions we determined the normalized (the maximum equals to 1) electron distribution functions in all three coordinates (Fig. 4a,b). For comparison in Fig. 4a the thermal distribution function with the temperature 66 MK is added. It shows that this distribution function has clear nonthermal tails. On the other hand, the computed distribution function in Fig. 4b is nearly the thermal one, see the fit of this function by the thick full line corresponding to the thermal distribution function with the temperature 107 MK.

In summary, Figs. 3 and 4 show that the successive merging (coalescences) of the plasmoids step by step increase the energy (and the temperature) of accelerated electrons. We found that at some regions and for short times during the coalescence process the distribution functions deviate from the thermal ones (the power-law tails in Fig. 4a or even bumps-on-tail, see e.g. Fig. 4 in the paper by Karlický & Bárta (2007)), but very soon these distribution functions are thermalized (i.e. changed to the Maxwellian ones) by fast wave-particle processes (anomalous collisions).

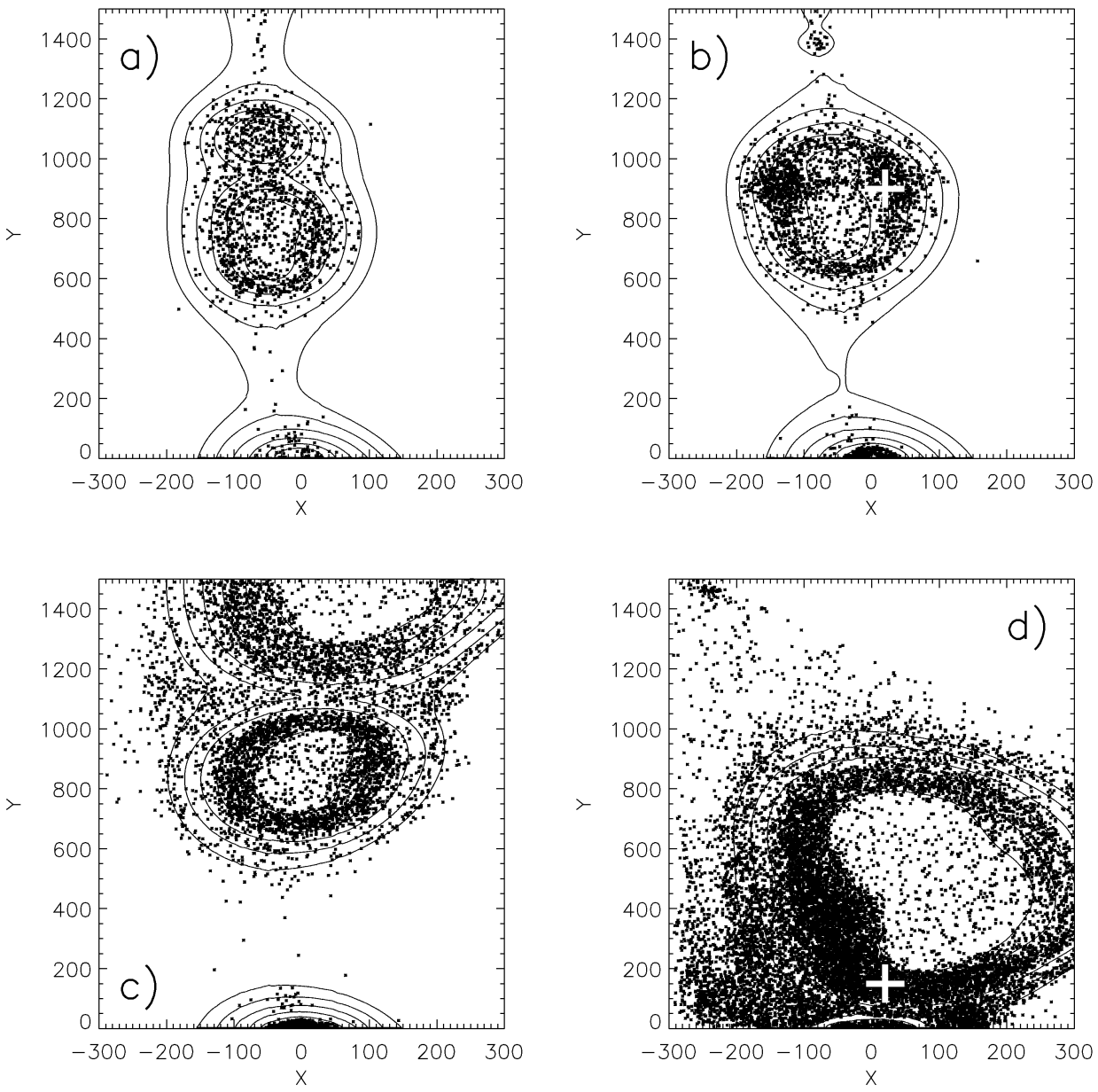

FIG. 3.— The detailed view on magnetic field lines in the $x - y$ computational plane and distribution of numerical electrons (points) having the energy greater than 40 keV at four different times: at $\omega_{pe}t = 3200$ (a), at $\omega_{pe}t = 3500$ (b), at $\omega_{pe}t = 5600$ (c), and at $\omega_{pe}t = 7800$ (d). The white crosses, located at b) x = 20, y = 900, and at d) x = 20, y = 150, show the regions where the distribution functions and the X-ray spectra were computed (see Figs. 4 and 5). The x and y coordinates are expressed in Δ.

3.1. *Successive merging of plasmoids and the above-loop-top hard X-ray sources*

We computed the hard X-ray spectra generated at two selected regions (the white crosses in Fig. 3) and compared them with that observed during the December 31, 2007 flare (Krucker et al. 2010). In accordance with the paper by Krucker et al. (2010) we have taken the plasma density in the range 10^9—10^{10} cm^{-3} and the source volume $V = 8\times\ 10^{26}$ cm^3. For the computation of the hard X-ray spectra we used two methods: (A) the non-thermal bremsstrahlung method, in which the spectrum was computed as a sum of contributions of the bremsstrahlung emission of all numerical electrons, for details see the relations (10) and (11) in the paper by Karlický & Kosugi (2004), and (B) the thermal bremsstrahlung method for specific plasma temperatures (Tandberg-Hanssen & Emslie 1988). The computed spectra together with the observed spectrum are in Fig. 5a,b. The spectra computed by the method (A) and (B) (in Fig. 5b) are similar. The observed spectrum is between the spectrum computed for the source plasma density 10^9 cm^{-3} and that for 10^{10} cm^{-3}, especially in later phases of the model evolution. But, the

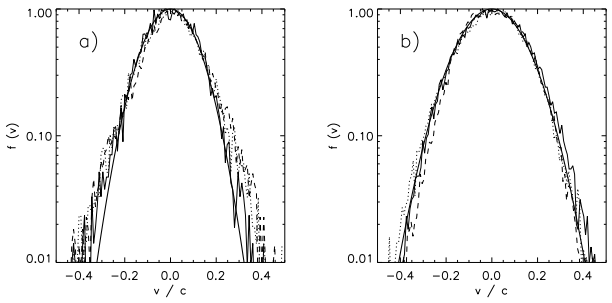

FIG. 4.— The normalized electron distribution functions (thin full line means f(v_x), dashed line f(v_y), and dotted line f(v_z)) computed in the regions shown by the white crosses in Fig. 3 at two different times: at $\omega_{pe}t = 3500$ (a) and at $\omega_{pe}t = 7800$ (b). The thick full line in (a) means the thermal distribution function with the temperature 66 MK and the thick full line in (b) the distribution function with the temperature 107 MK, which roughly fits the computed distribution functions.

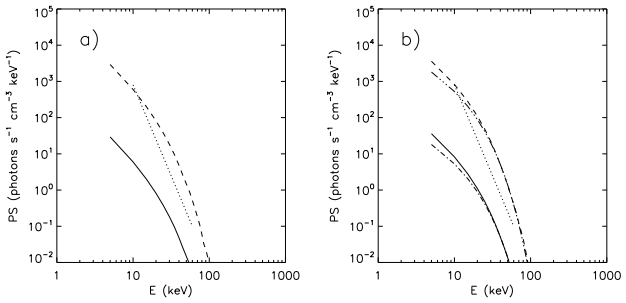

FIG. 5.— The X-ray spectra (a,b) (the full line for the source density $n_e = 10^9$ cm^{-3}, and the dashed line for $n_e = 10^{10}$ cm^{-3}) corresponding to the distributions in Fig. 4a, b, computed by method (A). The X-ray spectra in (b) (the dashed-dot line for the source density $n_e = 10^9$ cm^{-3}, and the dashed-dot-dot-dot line for $n_e = 10^{10}$ cm^{-3}) corresponding to the distribution in Fig. 4b, but computed by the method (B) for the temperature 107 MK. For comparison the X-ray spectrum (dotted line) observed during the December 31, 2007 flare (according to Krucker et al. 2010) is added.

observed spectrum has a different form, comparing to the computed ones. Considering our results we think the observed X-ray power-law spectrum is given by a sum of emissions from many locations with different thermal and nonthermal distribution functions.

3.2. *Fragmentation between merging plasmoids and narrowband dm-spikes*

In accordance with the results presented by Bárta et al. (2010b), we studied the structure of the magnetic field in the region between merging large plasmoids. One example of such a structure, formed at the time $\omega_{pe}t = 7200$ is presented in Fig. 6. The reddish areas mean the electric current densities with the initial orientation of the electric current, and the blue ones mean those with the opposite orientation; red and green lines are positions of $B_y = 0$ and $B_x = 0$, respectively; their intersections represent the X- and O- type null points. The figure shows that the initial current sheet is fragmented into several sub-current sheets. In these secondary current sheets further tearing can exist provided they are sufficiently long. Our results thus indicate, that the fragmentation cascade seen in a large-scale MHD simulation (Bárta et al. 2010b) continues actually down to the dissipation scale of the order $\approx d_i$ (the thickness of the CS at the bottom panel of Fig. 6 is $\approx 30\Delta$). At this scale, however no further fragmentation has been observed, the current structures dissipate by plasma kinetic processes 'silently'.

Considering the structures of fragmented current sheets (cascade of plasmoids) obtained by numerical simulations (Fig. 6), we constructed the schematic structure of fragmentation. An example of such a structure is shown in Fig. 7. The circles mean plasmoids with positively (+) and negatively (−) oriented electric currents, the parallel lines mean boundaries of current sheets. In such a structure the radius of the plasmoid R_i can be written as:

$$R_i = AR_{i+1} + BR_{i+2}, \tag{1}$$

where A and B are the numbers of plasmoids and current sheets in specific current sheet, i means the index of the plasmoids with the same size. The number of plasmoids increases with i as $n_i \sim \mathrm{B}^i$. Then, the ratio between subsequent radii of plasmoids in the plasmoid cascade can be expressed by the infinite continued fraction:

$$\frac{R_i}{R_{i+1}} = \left(A + \frac{B}{A + \frac{B}{A + \frac{B}{A+\ldots}}} \right). \tag{2}$$

Now, assuming that the energy in the plasmoids is proportional to their area, the dependence of the function $E_i = \mathrm{R}_i^2 \times \mathrm{n}_i$ on the k-vector scale ($k_i = 2\pi/\mathrm{R}_i$) can be computed. This function is the power-law one with the power-law index

$$p = \frac{\log(C \cdot B)}{\log \frac{R_i}{R_{i+1}}} - 2, \tag{3}$$

where C is the free parameter expressing possible deviations from our assumption about the plasmoid energy. For the structure presented in Fig. 7 and for $C = 1$ this power-law index is $p = -1.54$.

The power-law dependence were found also in the analysis of the frequency bandwidth of the narrowband dm-spikes (Karlický et al. 1996, 2000). Therefore, considering this fact, the model scenario shown in Fig. 1, and the turbulent-plasma model of spikes by Bárta & Karlický (2001), we propose that the narrowband dm-spikes are generated in fragmentation processes between merging plasmoids in the reconnection outflow in the region above the flare loop arcade. While Bárta & Karlický (2001) supposed (silently) MHD/Alfvénic turbulence in the super-sonic outflows, our recent simulations indicate that the tearing/coalescence cascade might be more likely source of turbulence. However, in a fully developed MHD turbulence all plasma wave-modes are present, anyway. In the fragmentation region, the plasmoids of all spatial scales can interact and accelerate electrons. These electrons are trapped in plasmoids of different sizes. In each plasmoid they can generate the radio emission in the frequency range corresponding to the range of the plasma density in this plasmoid. Due to expected power-law dependence of spatial scales of these fragmented plasmoids, the dependence of bandwidths of

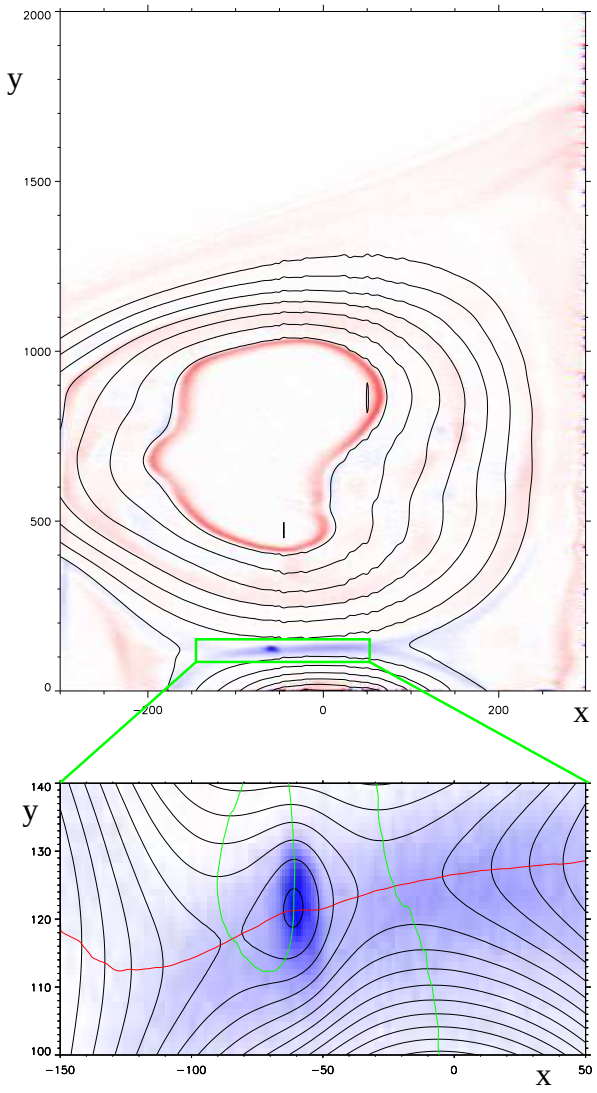

FIG. 6.— Fragmentation of the current sheet in the direction perpendicular to the initial current layer, i.e. in the current sheet between two large interacting plasmoids, at $\omega_{pe}t = 7200$. The reddish areas mean the electric current densities with the initial orientation of the electric current, and the blue ones mean those with the opposite orientation; red and green lines are positions of $B_y = 0$ and $B_x = 0$, respectively; their intersections represent the X- and O- type null points.

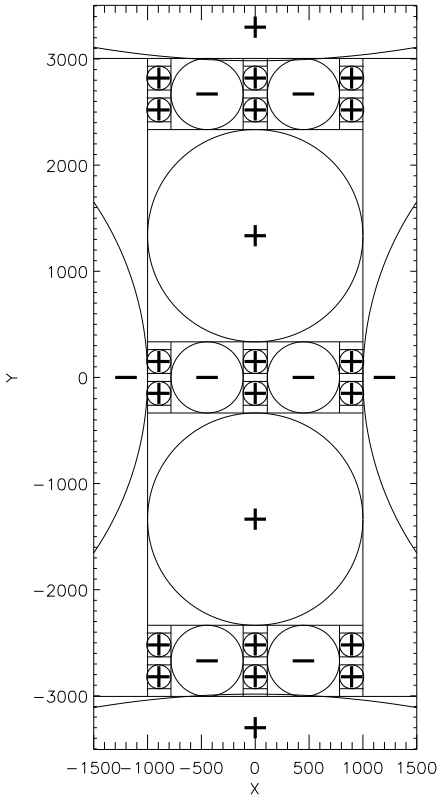

FIG. 7.— Example of the fractal reconnection structure corresponding to the relations (1) and (2), for A=2 and B=3. Double straight lines delineate current sheets with interacting plasmoids (circles). The plus and minus signs express orientation of electric currents in the plasmoids. X and Y are in arbitrary units.

the resulting radio emission should be the power-law one as observed in the narrowband dm-spikes.

To support this idea, in Fig. 8 we present the radio spectrum observed during the 28 March 2001 flare by two Ondřejov radiospectrographs (0.8—2.0 and 2.0—4.5 GHz) (Jiřička et al. 1993). It shows two positively drifting pulsating structures (DPSs) which according to our previous studies indicate two plasmoids moving downwards to the sources of the narrowband dm-spikes (generated in the region of fragmentation, compare to the model scenario in Fig. 1). The mean Fourier spectrum of these spikes is the power-law one with the power-law index −1.5.

4. DISCUSSION AND CONCLUSIONS

Important aspect of our model is that we used free boundary conditions which enabled successive merging of small plasmoids into a large final plasmoid. In simulations, we recognized also a fragmentation of current sheet between two merging plasmoids.

We showed that these processes very efficiently accelerate electrons to energies relevant for the emission in the hard X-ray range. Based on this result we propose that the above-the-loop-top hard X-ray sources are produced by the successive merging of plasmoids in the region with the turbulent reconnection outflow, in the region just above the loop arcade. Computed X-ray spectra support this idea. To explain a difference between the slopes of the computed and observed X-ray spectra we propose that the observed power-law spectrum is a sum of emissions from many locations with different thermal and nonthermal distribution functions.

In simulations we used the particle-in-cell model. Although, the studied processes are self-similar (i.e. they does not depend on scales, see e.g. the MHD and PIC simulations in the paper by Tajima et al. (1987)), the results need to be taken with a caution, because the spatial and time scales in the model and real plasmoids differ in several orders of magnitude. On the other hand, it is beyond a possibility of any present numerical model to take into account all these scales.

Further aspect of the PIC modelling is that the

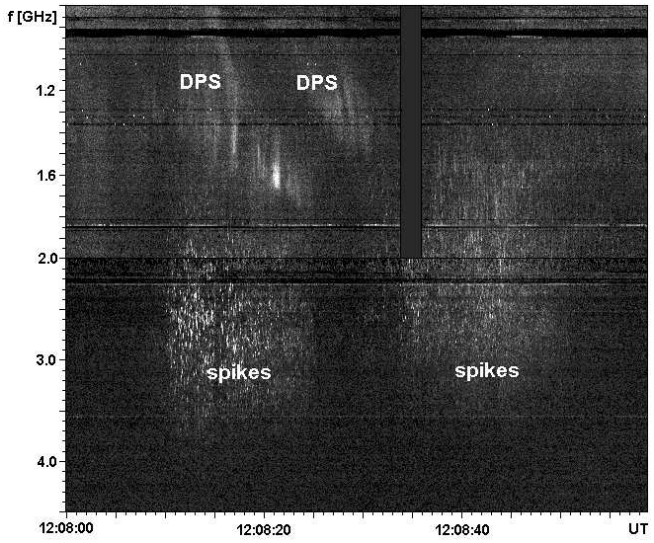

FIG. 8.— The radio spectrum observed during the 28 March 2001 flare by two Ondřejov radiospectrographs (0.8–2.0 and 2.0–4.5 GHz) supporting our model. It shows the drifting pulsating structures (DPSs) which drift towards narrowband dm-spikes. The 0.8–2.0 GHz spectrum was shortly interrupted at 12:08:34–12:08:36 UT.

Coulomb collisions were not considered in our model. Namely, the time interval of our computations is much shorter than the collision time in the-above-the-loop-top X-ray sources; e.g. $\omega_{pe}t = 7800$ for the plasma density $n_e = 10^9$ cm^{-3} corresponds to 4.5×10^{-6} s and the collision time to 0.115 $T_7^{3/2}$ s, where $T_7 = T_e/10^7$. On the other hand, the Coulomb collisions are essential for the bremsstrahlung X-ray emission. The hard X-ray spectra in the December 31, 2007 flare were detected as the mean ones over intervals of several seconds. Furthermore, the-above-the-loop-top hard X-ray source lasted of about 2 minutes. Thus comparing these times with the collision one, the collisions influence not only the observed spectra, but also a duration of the X-ray source. Therefore some re-acceleration of electrons is even needed. In the present model such a re-acceleration is very probable, because the plasmoids are generated in a broad range of spatial scales and electrons can travel several times though regions of interacting plasmoids. Although an inclusion of the Coulomb collisions and corresponding prolongation of computations are beyond the possibility of our present PIC modelling, we think that the observed spectra are given by a competition of the collisions with the re-acceleration of electrons. On the other hand, in PIC model the anomalous collisions (wave-particle interactions), which are much more effective than the Coulomb collisions, are present as confirmed by fast thermalization of nonthermal distribution functions.

We made additional computations with different initial parameters and we found: a) the energy gain of accelerated electrons increases with the decrease of the plasma beta parameter, and b) the increase of the proton-electron mass ratio m_p/m_e makes computations longer, but results are similar.

We compared the present simulation also with that in the numerical model which size was two times smaller ($L_x \times L_y = 600\Delta \times 2000\Delta$) and in which only 5 plasmoids were initiated (contrary to 10 plasmoids in the present simulation). In this case the final mean energy of accelerated electrons was 5.3 times greater than the initial one, compare with that of 10.7 times (from the initial temperature 10 MK to final temperature 107 MK) in the present case. Namely, each coalescence process increases the energy of accelerated electrons, therefore the number of successive coalescence processes is essential for their final energy.

For calculations of the hard X-ray spectra, presented in Fig. 5b we used two methods. The obtained results are similar. Small differences are due to differences in these methods and deviations of the computed distribution functions from the thermal one.

The plasmoids in 2-D are in reality 3-D magnetic ropes. While in 2-D the trapping of energetic electrons is a natural consequence of a close magnetic field structure of the plasmoid, in 3-D, this structure is only semi-closed. However, we consider the merging processes in the turbulent reconnection outflow therefore the magnetic trapping of electrons, similar to that proposed by Jakimiec et al. (1998) is highly probable. Moreover, the coalescence fragmentation process, which generates the reverse electric currents (which in 3-D has to be closed in finite volume) will contribute to a full trapping of electrons.

In agreement with the conclusions by Krucker et al. (2010), in the model the acceleration region is very close to the hard X-ray source. It enables to re-accelerate energetic electrons, which loss their energy due to collisions. Acceleration regions are among interacting plasmoids and also between the plasmoids and the arcade of flaring loops. This model can explain not only the above-the-loop-top hard X-ray sources, but also the loop-top sources because the arcade of loops is, in principle, the 'plasmoid' fixed in its half height at the photosphere.

Considering all aspects of the fragmentation process (power-law spatial scales of plasmoids, effective acceleration of electrons, trapping of electrons in plasmoids, location in the reconnection plasma outflow) we think that this process can explain a generation of the narrowband dm-spikes. We supported this idea by the radio spectrum observed during the 28 March 2001 showing DPSs drifting towards the narrowband dm-spikes. Furthermore, it is known that more than 70 % of all groups of dm-spikes are observed during the GOES-rising-flare phases (Jiřička et al. 2001). Although these arguments support the presented idea, further analysis of the narrowband dm-spikes and their modelling is necessary.

In this first study, we considered only the neutral current sheet, i.e. $B_z = 0$. For more realistic description, we plan to extend our study also to cases with non-zero guiding magnetic field.

The presented model is a natural extension of our previous models explaining the plasmoid formation, its ejection, and corresponding DPS. The question arises why the above-the-loop-top hard X-ray sources are very rare comparing, e.g., with DPSs or dm-spikes observations. We think that the above-the-loop-top hard X-ray source is large and stationary plasmoid, which is sufficiently dense and in which there is sufficient amount of energetic electrons. Positional stationarity and location of this plasmoid is given by surrounding magnetic field and

location where this plasmoid starts to be formed, see the paper by Bárta et al. (2008b). On the other hand, the plasmoids generating DPSs or dm-spikes need not to be so dense and they need not to have such amount of energetic electrons. It is known that for generation of the radio emission a number of energetic electrons can be much smaller than that for the hard X-ray emission. Namely, the intensity of the radio emission depends on derivatives of the electron distribution function in the momentum space; not on the absolute amount of energetic electrons as in the case of the hard X-ray emission.

This research was supported by Grant IAA300030701 of the Grant Agency of the Academy of Sciences of the Czech Republic and the research project AV0Z10030501 of Astronomical Institute of the Czech Academy of Science.

REFERENCES

Aschwanden, M.J. 1990, Astron. Astrophys. Suppl., 85, 1141
Bárta, M., Büchner, J., & Karlický, M. 2010a, Adv. Space Res., 45, 10
Bárta, M., Büchner, J., Karlický, M., & Skála, J. 2010b, ApJ, submitted, 2010, arXiv:1011.4035B
Bárta, M., & Karlický, M. 2001, A&A, 379, 1045
Bárta, M., Karlický, M., & Žemlička, R. 2008a, Sol. Phys., 253, 173
Bárta, M., Vršnak, B., & Karlický, M. 2008b, A&A, 477, 649
Benz, A.O. 1986, Sol. Phys., 104, 99
Benz, A.O., Zlobec, P., & Jaeggi, M. 1982, A&A, 109, 305
Drake, J.F., Scudder, J., & Karimabadi, H. 2006, Phys. Plasmas, 13, 072101
Drake, J.F., Shay, M.A., Thongthai, W., & Swisdak, M. 2005, Phys. Rev. Letters, 94, 095001
Fleishman, G.D. & Yastrebov, S.G. 1994, Sol. Phys., 154, 361
Fletcher, L. 2004, A&A, 303, L9
Fu, Q.J., Li, C.S., & Yin, S.Z. 1985, in C. de Jager and Chen Biao (eds.), Kunming Workshop on Solar Physics and Interplanetary travelling phenomena, Science Press, Beijing, p. 560
Güdel, M. 1990, A&A, 239, L1
Güdel, M., & Zlobec, P. 1991, A&A, 299
Holman, G.D., Eichler, D., & Kundu, M. 1980, in M. Kundu and T. Gergely (eds.), IAU Symp. 86, 465
Hoshino, M. 2005, J. Geophys. Res., 106, 25979
Jakimiec, J., Tomczak, M., Falewicz, R., Phillips, K.J.H., & Fludra, A. 1998, A&A, 334, 1112
Jiřička, K., Karlický, M., Kepka, O., & Tlamicha, A. 1993, Sol. Phys., 147, 203
Jiřička, K., Karlický, M., Mészárosová, H., & Snížek, V. 2001, A&A, 375, 243
Karlický, M. 1984, Sol. Phys., 92, 329
Karlický, M. 2004, A&A, 417, 325
Karlický, M. 2008, ApJ, 674, 1211
Karlický, M., & Bárta, M. 2007, A&A, 464, 735
Karlický, M., Bárta, M., & Rybák, J. 2010, A&A, 514, id.A28
Karlický, M., Fárník, F., & Mészárosová, H. 2002, A&A, 395, 677
Karlický, Jiřička, K., & Sobotka, M. 2000, Sol. Phys., 195, 165
Karlický, M., & Kosugi, T. 2004, A&A, 419, 1159
Karlický, M., Sobotka, M.,& Jiřička, K. 1996, Sol. Phys., 168, 375
Kliem, B., Karlický, M., & Benz, A. O. 2000, A&A, 360, 715
Kolomanski, S., & Karlický, M. 2007, A&A, 475, 685
Krucker, S. & Benz, A.O. 1994, A&A, 285, 1038
Krucker, S., Hudson, H.S., Glesener, L., White, S.M., Masuda, S., Wuelser, J.P. & Lin, R.P 2010, ApJ, 714, 1108
Krucker, S., & Lin, R.P. 2008, ApJ, 673, 1181
Kuijpers, J., Van der Post, P., & Slottje, C. 1981, A&A, 102, 331
Loureiro, N. F., Schekochihin, A. A., & Cowley, S. C. 2007, Physics of Plasmas, 14, 100703, arXiv:astro-ph/0703631
Magara, T., Mineshige, S., Yokoyama, T.,& Shibata, K. 1996, ApJ, 466, 1054
Masuda, S., Kosugi, T., Hara, H., Tsuneta, S., & Ogawara, Y. 1994, Nature, 371, 495
Melrose, D.B., & Dulk, G.A. 1982, ApJ, 259, 844
Mészárosová, H., Veronig, A., Zlobec, P., & Karlický, M. 2003, A&A, 407, 1115
Milligan, R.O., McAteer, R.T.J., Dennis, B.R., & Young, C. A. 2010, ApJ, 713, 1292
Ohyama, M., & Shibata, K. 1998, ApJ, 499, 934
Oka, M., Phan, T.D., Krucker, S., Fujimoto, M., & Shinohara, I. 2010, ApJ, 714, 915
Park, S.H., & Fleishman, G. D. 2010, Sol. Phys., 266, 323
Petrosian, V., Donaghy, T.Q., & McTierman, J.M. 2002, ApJ, 569, 459
Pritchett, P.L. 2006, J. Geophys. Res., 111, A10212
Pritchett, P.L. 2008, Phys. Plasmas, 15, 102105
Saito, S., & Sakai, J.I. 2004, ApJ, 616, L179
Shibata, K., & Tanuma, S. 2001, Earth Planets Space, 53, 473
Slottje, C. 1981, Atlas of Fine Structures of Dynamic Spectra of Solar Type IV-dm and Some Type II Radio Bursts, Dwingeloo Observatory
Stähli, M., & Magun, A. 1986, Sol. Phys., 104, 117
Tajima, T., Benz, A.O., Thaker, M., & Leboeuf, J.N. 1990, ApJ, 353, 666
Tajima, T., Sakai, J., Nakajima, H., Kosugi, T., Brunel, F., & Kundu, M.R. 1987, ApJ, 321, 1031
Tandberg-Hanssen, E., & Emslie, A.G. 1988, The Physics of Solar Flares, Cambridge University Press, Cambridge, UK
Tomczak, M. 2001, A&A, 366, 294
Uzdensky, D. A., Loureiro, N. F., & Schekochihin, A. A. 2010, Physical Review Letters, 105, 235002, 1008.3330
Veronig, A., & Brown, J.C. 2004, ApJ, 663, L117
Vlahos, L., & Sharma, R.R. 1984, ApJ, 290, 347
Wentzel, D.G. 1991, ApJ, 373, 285
Winglee, R.R., Dulk, G.A., & Pritchett, P.L. 1988, ApJ, 328, 809
Zlobec, P., & Karlický, M. 1998, Sol. Phys., 182, 477